Vera Erbes, Stefan Weinzierl, Sascha Spors

Evanescent Aliasing of Virtual Sources close to a Wave Field Synthesis Array

Erbes, Vera; Weinzierl, Stefan; Spors, Sascha (2015): Evanescent Aliasing of Virtual Sources close to a Wave Field Synthesis Array . In: Fortschritte der Akustik - DAGA 2015: 41. Jahrestagung für Akustik, 16. - 19. März 2015 in Nürnberg. Berlin: Deutsche Gesellschaft für Akustik e.V. pp. 494–497.

Evanescent Aliasing of Virtual Sources close to a Wave Field Synthesis Array

Vera Erbes[1], Stefan Weinzierl[1], Sascha Spors[2]

[1] *Audio Communication Group, TU Berlin, Germany, Email: {v.erbes, stefan.weinzierl}@tu-berlin.de*

[2] *Institute of Communications Engineering, Universität Rostock, Germany, Email: sascha.spors@uni-rostock.com*

Introduction

Positioning virtual sources close to the discrete secondary sources of a wave field synthesis array leads to amplitude deviations of the synthesised field. The field of a virtual source right behind or in front of a secondary source is amplified, while the field of a virtual source between two secondary sources is attenuated [1]. This paper analyses this effect in terms of spatial aliasing which originates from the discretisation of the secondary source distribution. While propagating spatial aliasing artefacts occur only above a certain frequency limit, evanescent aliasing is always present in the synthesised field [2]. The evanescent components decay rapidly at small distances from the secondary sources. This is not the case for virtual sources close to the secondary sources. It is shown that the observed change in amplitude is caused by evanescent aliasing. The paper treats both virtual point sources and focused sources for driving functions derived by the spectral division method (SDM) as well as wave field synthesis (WFS) driving functions for a linear array.

Amplitude deviations

The amplitude deviations for virtual point sources close to discrete secondary point sources is shown in fig. 1 for a virtual source right behind a secondary source at $\mathbf{x}_{\mathrm{ps}} = (x_{\mathrm{ps}}, y_{\mathrm{ps}}, 0) = (0,\ -0.02,\ 0)$ m. The target sound field is

$$S(\mathbf{x}, \omega) = \hat{S}_{\mathrm{ps}}(\omega) \cdot \frac{\mathrm{e}^{\mathrm{j}\frac{\omega}{c}|\mathbf{x}-\mathbf{x}_{\mathrm{ps}}|}}{|\mathbf{x}-\mathbf{x}_{\mathrm{ps}}|} \tag{1}$$

with signal amplitude $\hat{S}_{\mathrm{ps}}(\omega) = \sqrt{2}$ Pa at 350 Hz. The virtual source is synthesised by SDM with a linear array. The secondary source spacing Δx_0 is 0.2 m throughout this paper. Compared to the real point source in fig. 1 (a) and (c), the synthesised sound field not only shows the expected 2.5D amplitude decay of approx. 3 dB per doubling of the distance. The amplitude and level in fig. 1 (b) and (d) are too high throughout the entire field and in particular not correct on the reference line in fig. 1 (b) and (d). Evaluating the level at a point on the reference line $\mathbf{x}_{\mathrm{ref}} = (0, 1, 0)$ yields 94 $\mathrm{dB_{SPL}}$ for the real and 104 $\mathrm{dB_{SPL}}$ for the virtual point source.

Analysis of spatial aliasing components

The observed amplitude error for a virtual point source synthesised by SDM with a linear array of secondary point sources will now be analysed in terms of spatial aliasing. The framework introduced in [3] is used. As [3] has covered the 2D case, the equations for 2.5D synthesis are derived here.

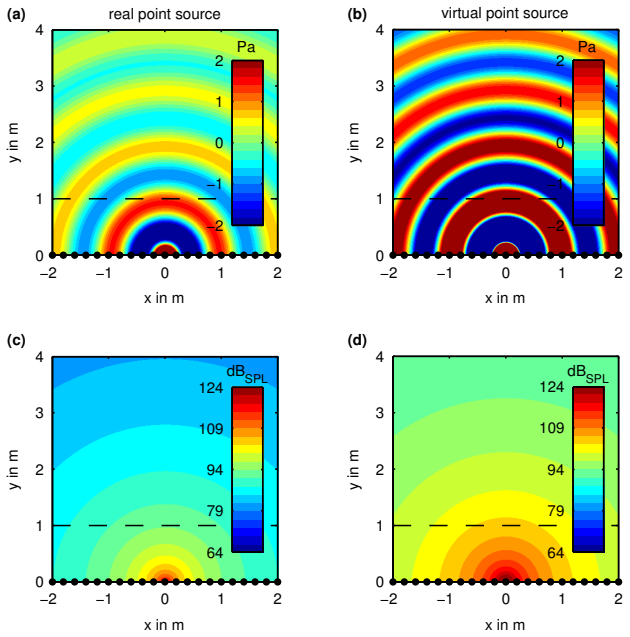

Figure 1: Sound field of a real (left) and a virtual (right) source at $\mathbf{x}_{\mathrm{ps}} = (0,\ -0.02,\ 0)$ m by SDM with a linear array of secondary point sources with $\Delta x_0 = 0.2$ m and $\hat{S}_{\mathrm{ps}}(\omega) = \sqrt{2}$ Pa at $f = 350$ Hz; a, b: real part, c, d: level. Dashed line: reference line, black dots: positions of secondary sources.

The spectrum of the 3D Green's function in free field evaluated in the x, y-plane in the spatio-temporal frequency domain reads [2]:

$$\tilde{G}_{0,3\mathrm{D}}(k_x, y, z=0, \omega) = \begin{cases} -\frac{\mathrm{j}}{4} H_0^{(2)}\left(\sqrt{\left(\frac{\omega}{c}\right)^2 - k_x^2} \cdot |y|\right) & , \quad |k_x| < \left|\frac{\omega}{c}\right| \\ \frac{1}{2\pi} K_0\left(\sqrt{k_x^2 - \left(\frac{\omega}{c}\right)^2} \cdot |y|\right) & , \quad \left|\frac{\omega}{c}\right| < |k_x| \end{cases} \tag{2}$$

with $H_0^{(2)}(\cdot)$ denoting the zeroth-order Hankel function of second kind, $K_0(\cdot)$ the zeroth order modified Bessel funcion of second kind, k_x the spatial frequency and c the speed of sound. The definition of the temporal and spatial Fourier transform are as in [2]. The spectrum is split up into a propagating part for $|k_x| < \left|\frac{\omega}{c}\right|$ and an evanescent part for $\left|\frac{\omega}{c}\right| < |k_x|$, which can be seen in fig. 2 (a) inside and outside the orange wegde, respectively.

For a virtual point source at the position $\mathbf{x}_{\mathrm{ps}} = (x_{\mathrm{ps}}, y_{\mathrm{ps}}, 0)$, $y_{\mathrm{ps}} < 0$, with the target sound field given in eq. (1), the spatio-temporal spectrum of the driving function can be derived by SDM. To facilitate the inverse spatial Fourier transform, two approximations are incorporated: The distances of the reference line to the

virtual point source and to the secondary sources (y_{ref}) have to be large compared to the signal wavelength. The resulting spectrum of the driving function then is [4]

$$\tilde{D}_{\mathrm{SDM,ps}}(k_x,\omega) = 4\pi \cdot \Delta x_0 \cdot \sqrt{\frac{y_{\mathrm{ref}}}{y_{\mathrm{ref}}-y_{\mathrm{ps}}}} \cdot \mathrm{e}^{\mathrm{j}k_x x_{\mathrm{ps}}} \times \cdot \begin{cases} \mathrm{e}^{\mathrm{j}\sqrt{\left(\frac{\omega}{c}\right)^2 - k_x^2}\cdot y_{\mathrm{ps}}} & , \quad |k_x| < \left|\frac{\omega}{c}\right| \\ \mathrm{e}^{\sqrt{k_x^2 - \left(\frac{\omega}{c}\right)^2}\cdot y_{\mathrm{ps}}} & , \quad \left|\frac{\omega}{c}\right| < |k_x| \end{cases} \tag{3}$$

for a secondary source distribution of point sources along the x-axis including weighting with the secondary source spacing Δx_0. The absolute value of $\tilde{D}_{\mathrm{SDM,ps}}(k_x,\omega)$ can be seen as the wegde centred at $k_x = 0$ in fig. 2 (b) without the other wegdes present. The spectrum can again be devided in a propagating part inside the red wegde and an evanescent part outside.

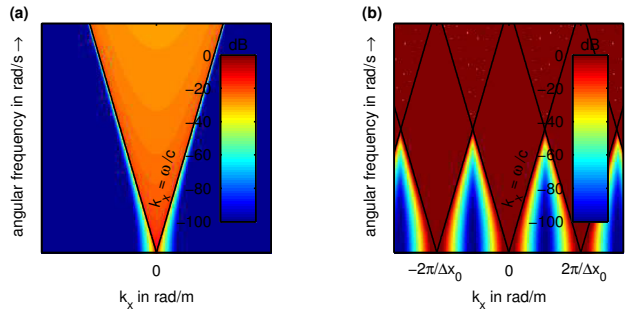

Figure 2: Magnitude spectra in the wavenumber domain, a: Green's function of a spherical monopole, b: repeated spectrum of the driving function

Discrete secondary sources

The discretisation of a secondary source distribution can be represented by multiplying the driving function $D(x_0,\omega)$ with a series of spatial Dirac functions. In the spatio-temporal frequency domain this yields [5]

$$\tilde{D}_{\mathrm{S}}(k_x,\omega) = \frac{1}{\Delta x_0} \cdot \sum_{\eta=-\infty}^{\infty} \tilde{D}\left(k_x - \frac{2\pi}{\Delta x_0}\eta, \omega\right). \tag{4}$$

This constitutes a repetition of the spectrum of the driving function along the k_x-axis with an interval of $\frac{2\pi}{\Delta x_0}$. Fig. 2 (b) shows $\tilde{D}_{\mathrm{S}}(k_x,\omega)$ for the driving function from eq. (3). The evanescent components are stronger for lower frequencies both for $\tilde{D}_{\mathrm{S}}(k_x,\omega)$ and $\tilde{G}_{0,\mathrm{3D}}(k_x,y,z=0,\omega)$ and none of these spectra is bandlimited.

Propagating and evanescent components

In the wavenumber domain the spectra of the Green's function and of the driving function are multiplied to derive the spectrum of the synthesised sound field $\tilde{P}(k_x,y,z=0,\omega)$ in the x,y-plane. Four different areas of overlap result when differentiating into propagating and evanescent parts.

Following [3], the propagating part of the spectrum of the secondary sources overlapping the propagating and evanescent parts of the driving function can be expressed by

$$\tilde{P}_{\mathrm{S,pr1}}(k_x,y,z=0,\omega) = -\mathrm{j}\pi \cdot \sqrt{\frac{y_{\mathrm{ref}}}{y_{\mathrm{ref}}-y_{\mathrm{ps}}}} \cdot H_0^{(2)}\left(\sqrt{\left(\frac{\omega}{c}\right)^2 - k_x^2}\cdot|y|\right) \times \cdot \sum_{\eta'} \mathrm{e}^{\mathrm{j}\left(k_x - \frac{2\pi}{\Delta x_0}\eta'\right)\cdot x_{\mathrm{ps}}} \cdot \mathrm{e}^{\mathrm{j}\sqrt{\left(\frac{\omega}{c}\right)^2 - \left(k_x - \frac{2\pi}{\Delta x_0}\eta'\right)^2}\cdot y_{\mathrm{ps}}} \tag{5}$$

for $|k_x| < \left|\frac{\omega}{c}\right|$ and all η' with $\left|k_x - \frac{2\pi}{\Delta x_0}\eta'\right| < \left|\frac{\omega}{c}\right|$, and

$$\tilde{P}_{\mathrm{S,pr2}}(k_x,y,z=0,\omega) = -\mathrm{j}\pi \cdot \sqrt{\frac{y_{\mathrm{ref}}}{y_{\mathrm{ref}}-y_{\mathrm{ps}}}} \cdot H_0^{(2)}\left(\sqrt{\left(\frac{\omega}{c}\right)^2 - k_x^2}\cdot|y|\right) \times \cdot \sum_{\eta'} \mathrm{e}^{\mathrm{j}\left(k_x - \frac{2\pi}{\Delta x_0}\eta'\right)\cdot x_{\mathrm{ps}}} \cdot \mathrm{e}^{\sqrt{\left(k_x - \frac{2\pi}{\Delta x_0}\eta'\right)^2 - \left(\frac{\omega}{c}\right)^2}\cdot y_{\mathrm{ps}}} \tag{6}$$

for $|k_x| < \left|\frac{\omega}{c}\right|$ and all η' with $\left|k_x - \frac{2\pi}{\Delta x_0}\eta'\right| > \left|\frac{\omega}{c}\right|$, respectively.

The overlaps of the evanescent part of the spectrum of the secondary sources with propagating and evanescent contributions of the driving function are expressed by

$$\tilde{P}_{\mathrm{S,ev1}}(k_x,y,z=0,\omega) = 2 \cdot \sqrt{\frac{y_{\mathrm{ref}}}{y_{\mathrm{ref}}-y_{\mathrm{ps}}}} \cdot K_0\left(\sqrt{\left(k_x^2 - \frac{\omega}{c}\right)^2}\cdot|y|\right) \times \cdot \sum_{\eta'} \mathrm{e}^{\mathrm{j}\left(k_x - \frac{2\pi}{\Delta x_0}\eta'\right)\cdot x_{\mathrm{ps}}} \cdot \mathrm{e}^{\mathrm{j}\sqrt{\left(\frac{\omega}{c}\right)^2 - \left(k_x - \frac{2\pi}{\Delta x_0}\eta'\right)^2}\cdot y_{\mathrm{ps}}} \tag{7}$$

for $|k_x| > \left|\frac{\omega}{c}\right|$ and all η' with $\left|k_x - \frac{2\pi}{\Delta x_0}\eta'\right| < \left|\frac{\omega}{c}\right|$, and

$$\tilde{P}_{\mathrm{S,ev2}}(k_x,y,z=0,\omega) = 2 \cdot \sqrt{\frac{y_{\mathrm{ref}}}{y_{\mathrm{ref}}-y_{\mathrm{ps}}}} \cdot K_0\left(\sqrt{\left(k_x^2 - \frac{\omega}{c}\right)^2}\cdot|y|\right) \times \cdot \sum_{\eta'} \mathrm{e}^{\mathrm{j}\left(k_x - \frac{2\pi}{\Delta x_0}\eta'\right)\cdot x_{\mathrm{ps}}} \cdot \mathrm{e}^{\sqrt{\left(k_x - \frac{2\pi}{\Delta x_0}\eta'\right)^2 - \left(\frac{\omega}{c}\right)^2}\cdot y_{\mathrm{ps}}} \tag{8}$$

for $|k_x| > \left|\frac{\omega}{c}\right|$ and all η' with $\left|k_x - \frac{2\pi}{\Delta x_0}\eta'\right| > \left|\frac{\omega}{c}\right|$, respectively.

Virtual point source at a distance to the secondary sources

Fig. 3 shows the sound field components described by eq. (5)–(8) for a virtual point source at $\mathbf{x}_{\mathrm{ps}} = (0, -1, 0)$ m. The chosen frequency of 350 Hz is below the spatial aliasing frequency for propagating aliasing [3], i.e. the desired propagating contribution for $\eta = 0$ is the only contribution in $P_{\mathrm{S,pr1}}$.

The other propagating part of the sound field, $P_{\mathrm{S,pr1}}$, is very small (cf. the different colorbar axes in fig. 3 (a)–(d)) because the evanescent contributions of the repeated

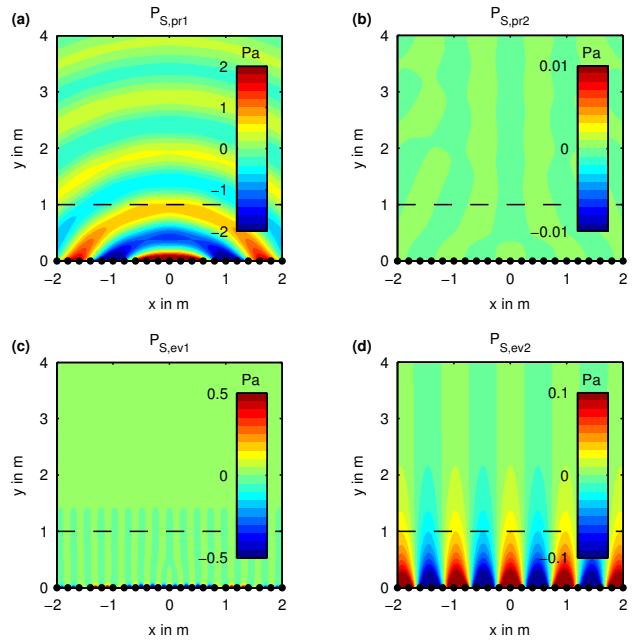

Figure 3: Sound field components according to eq. (5)–(8) in figure (a)–(d) for a virtual source at $\mathbf{x}_{\mathrm{ps}} = (0, -1, 0)$ m with $\Delta x_0 = 0.2$ m and $\hat{S}_{\mathrm{ps}}(\omega) = \sqrt{2}$ Pa at $f = 350$ Hz.

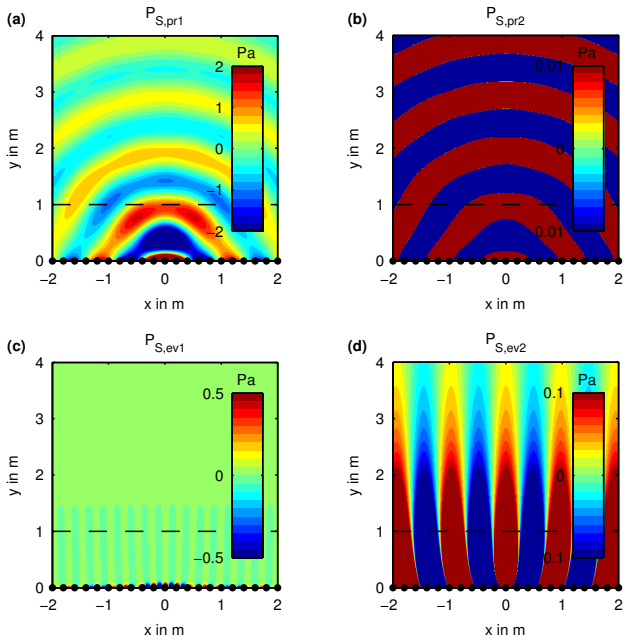

Figure 4: Sound field components according to eq. (5)–(8) in figure (a)–(d) for a virtual source at $\mathbf{x}_{\mathrm{ps}} = (0, -0.02, 0)$ m with $\Delta x_0 = 0.2$ m and $\hat{S}_{\mathrm{ps}}(\omega) = \sqrt{2}$ Pa at $f = 350$ Hz.

spectra of the driving functions reaching into the propagating part of the secondary sources have already decayed to a very low level. Similarly, $P_{\mathrm{S,ev1}}$ is neglectable as the spectrum of the Green's function is decaying fast enough for larger $|k_x|$.

The last part $P_{\mathrm{S,ev2}}$, where evanescent components of driving functions and secondary sources overlap, contains mostly the desired proportion for $\eta = 0$ due to the rapid decay of the evanescent components.

Virtual point source close to the secondary sources

The sound field components for a virtual point source close to the secondary sources at $\mathbf{x}_{\mathrm{ps}} = (0, -0.02, 0)$ m are depicted in fig. 4. $P_{\mathrm{S,pr2}}$ is now amplified because the evanescent parts of the driving function increase and have a great impact by overlapping with the propagating part of the spectrum of the secondary sources. This constitutes a propagating wave emerging from evanescent aliasing. Note that the shape of the wave fronts is very similar to $P_{\mathrm{S,pr1}}$. In addition, $P_{\mathrm{S,ev2}}$ is increased as well, which is a combination of evanescent aliasing and a reconstruction error. $P_{\mathrm{S,pr2}}$ and $P_{\mathrm{S,ev2}}$ together preserve the shape of the field from the virtual point source, though.

In contrast, when placing the virtual source not directly behind a secondary source, but between them, the amplitude of the resulting wave field is strongly attenuated. Though not shown here, this again is caused by $P_{\mathrm{S,pr2}}$ that is inverted in phase compared to the desired wave fronts. Correspondingly, the accompanying contribution $P_{\mathrm{S,ev2}}$ for $\eta \neq 0$ is inverted as well. Thus, the amplitude of the resulting total sound field is diminished.

Focused source close to the secondary sources

For a focused source at $\mathbf{x}_{\mathrm{fs}} = (x_{\mathrm{fs}}, y_{\mathrm{fs}}, 0)$ with $y_{\mathrm{fs}} > 0$ synthesised with a driving function equivalent to eq. (3) the result is directly comparable. The amplitude deviations on the reference line can again be explained by the increased amount of evanescent components of the driving function that are in- or out-of-phase depending on the position of the focused source with respect to the x-axis, i.e. directly in front of or between secondary sources.

Evanescent Aliasing in WFS

In comparison to the driving function derived by SDM, the WFS driving function for a virtual point source [4]

$$D_{\mathrm{WFS,ps}}(x_0, \omega) = -4\pi \cdot \Delta x_0 \cdot \sqrt{\mathrm{j}\frac{\omega}{c}} \cdot \sqrt{\frac{y_{\mathrm{ref}}}{y_{\mathrm{ref}} - y_{\mathrm{ps}}}} \times \cdot \frac{y_{\mathrm{ps}}}{|\mathbf{x_0} - \mathbf{x}_{\mathrm{ps}}|} \cdot \frac{\mathrm{e}^{-\mathrm{j}\frac{\omega}{c}|\mathbf{x_0} - \mathbf{x}_{\mathrm{ps}}|}}{\sqrt{|\mathbf{x_0} - \mathbf{x}_{\mathrm{ps}}|}} \tag{9}$$

is subject to an additional approximation requiring a large distance of the virtual point source to the secondary source distribution compared to the signal wavelength. A virtual source positioned as in fig. 4 is clearly violating this condition. The resulting amplitude of the reproduced field is then too small as shown in fig. 5. This is counteracting the amplitude increase for virtual sources directly behind and further diminishing the amplitude for virtual sources between secondary sources.

Limits of evanescent aliasing

No exact limit can be given for evanescent aliasing as the spectrum of the driving function is not bandlimited.

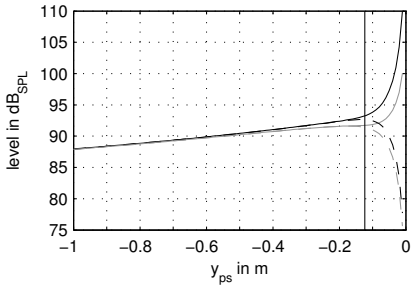

Figure 5: Level at $\mathbf{x}_{\mathrm{ref}} = (0,\ 1,\ 0)$ m of a virtual point source over distance y_{ps} with $\Delta x_0 = 0.2$ m and $\hat{S}_{\mathrm{ps}}(\omega) = \sqrt{2}$ Pa at $f = 350$ Hz. Black: SDM, grey: WFS. Solid lines: virtual source right behind ($x_{\mathrm{ps}} = 0$), dashed lines: virtual source between secondary sources ($x_{\mathrm{ps}} = 0.1$ m). Vertical line: distance to avoid evanescent aliasing after criterion in eq. (11).

The effect becomes more pronounced at lower frequencies. To reduce it, the virtual point source has to be far enough away from the secondary sources. The contribution of the undesired evanescent components of the repeated spectrum of the driving function overlapping the spectrum of the Green's function should be small compared to the desired sound field components for $\eta = 0$. A derivation out of the corresponding equations is not straightforward. Therefore, an approximated criterion is proposed, derived from eq. (3) and (4).

To keep the evanescent aliasing artefacts within bounds, only the most prominent contributions are considered. Thus, it is sufficient to take only one of the first repetitions of the spectrum of the driving function into account. Furthermore, only the overlap with the propagating part of the Green's function is considered as this contribution generates the additional propagating wave fronts. The condition for the remaining evanescent contribution of the driving function for the first repetition for $\eta = 1$ overlapping the propagating part of the Green's function to be small compared to the propagating part of the driving function for $\eta = 0$, can be expressed as

$$\mathrm{e}^{\sqrt{\left(k_x - \frac{2\pi}{\Delta x_0}\right)^2 - \left(\frac{\omega}{c}\right)^2}\cdot y_{\mathrm{ps}}} \ll a \qquad (10)$$

for $0 < a < 1$. To take the frequency dependency into account caused by the higher magnitude of the propagating spectrum of the Green's function at lower frequencies, eq. (10) is evaluated at $k_x = -\left|\frac{\omega}{c}\right|$. Thus, a comparable frequency dependency is induced as generated by the Hankel function in eq. (2). This leads to the criterion for the distance y_{ps} of the virtual source to the secondary sources

$$y_{\mathrm{ps}} \ll \frac{\ln(a)}{\sqrt{\frac{2\pi}{\Delta x_0}\left(\frac{2\pi}{\Delta x_0} + \frac{\omega}{c}\right)}}. \qquad (11)$$

Note that $y_{\mathrm{ps}} < 0$ here. For $a = 0.01$, the resulting limit is shown in fig. 5 as a vertical line.

Discussion

While the driving function is calculated based on spherical monopole sources as secondary sources, loudspeakers are better modelled as a baffled circular piston [6]. As the analysed effect of evanescent aliasing is mostly relevant at low frequencies and the qualitative behaviour of the spatio-temporal spectrum of a baffled circular piston is well approximated by a spherical monopole at low frequencies, the described amplitude deviation can be expected to occur in practice as well.

To reduce the amplitude deviations, driving functions for virtual sources close to a discrete secondary source distribution could be treated differently. Limiting the amplification factor for close virtual sources, as implemented in the SoundScape Renderer [7] to avoid excessive gain, will reduce the effect. In [1], an oversampling and averaging approach for the driving function is proposed to reduce the differences between virtual sources right behind/in front of and between secondary sources.

Conclusions

The amplitude deviations at the reference point of virtual point and focused sources close to a discrete secondary source distribution synthesised by SDM and WFS have been analysed. This has been done by separating the sound field in propagating and evanescent parts. It has been shown that the deviations are caused by the evanescent part of the repeated spectrum of the driving function overlapping the spectrum of the Green's function, thus constituting evanescent aliasing. A criterion has been derived for the minimum distance of a virtual source to the secondary sources to reduce the amplitude errors.

References

[1] Lee, J.-M., Choi J.-W., Kim Y.-H.: Wave field synthesis of a virtual source located in proximity to a loudspeaker array. J. Acoust. Soc. Am 134 (2013), 2106–2117

[2] Ahrens, J., Spors S.: Sound Field Reproduction Using Planar and Linear Arrays of Loudspeakers. IEEE Trans. on Audio, Speech, and Language Processing 18 (2010), 2038–2050

[3] Spors, S., Ahrens, J.: Spatial Sampling Artifacts of Wave Field Synthesis for the Reproduction of Virtual Point Sources. Proc. of the 126th AES Convention 2009

[4] Spors, S., Ahrens, J.: Analysis and Improvement of Pre-equalization in 2.5-Dimensional Wave Field Synthesis. Proc. of the 128th AES Convention 2010

[5] Schultz, F., Rettberg T., Spors S.: On Spatial-Aliasing-Free Sound Field Reproduction using Infinite Line Source Arrays. Proc. of the 136th AES Convention 2014

[6] Blackstock, D. T.: Fundamentals of Physical Acoustics. Wiley, New York, 2000

[7] SoundScape Renderer, URL: `http://spatialaudio.net/ssr/`